Brain Research Bulletin 207 (2024) 110877

Contents lists available at ScienceDirect

Brain Research Bulletin

journal homepage: www.elsevier.com/locate/brainresbull

Research report

# Nrf-2 modulates excitability of hippocampal neurons by regulating ferroptosis and neuroinflammation after subarachnoid hemorrhage in rats

Dazhao Fang [a,b], Shenquan Guo [a], Boyang Wei [a], Wenchao Liu [a], Guangxu Li [a], Xifeng Li [a], Jiahui Liu [a], Lei Jin [a], Chuanzhi Duan [a,*]

[a] Neurosurgery Center, Department of Cerebrovascular Surgery, Engineering Technology Research Center of Education Ministry of China on Diagnosis and Treatment of Cerebrovascular Disease, Zhujiang Hospital, Southern Medical University, Guangzhou, Guangdong, China
[b] Department of Neurosurgery, The Affiliated Huaian No.1 People's Hospital of Nanjing Medical University, Huaian, Jiangsu, China

ARTICLE INFO

*Keywords:*
Nuclear factor E2-related factor (Nrf-2)
Neural excitability
Ferroptosis
Subarachnoid hemorrhage (SAH)
Neuroinflammation

ABSTRACT

Excitability of hippocampal neurons in subarachnoid hemorrhage (SAH) rats has not been well studied. The rat SAH model was applied in this study to explore the role of nuclear factor E2-related factor (Nrf-2) in the early brain injury of SAH. The neural excitability of CA1 pyramidal cells (PCs) in SAH rats was evaluated by using electrophysiology experiments. Ferroptosis and neuroinflammation were measured by ELISA, transmission electron microscopy and western blotting. Our results indicated that SAH induced neurological deficits, brain edema, ferroptosis, neuroinflammation and neural excitability in rats. Ferrostatin-1 treatment significantly decreased the expression and distribution of IL-1β, IL-6, IL-10, TGF-β and TNF-α. Inhibiting ferroptosis by ferrostatin-1 can attenuate neural excitability, neurological deficits, brain edema and neuroinflammation in SAH rats. Inhibiting the expression of Nrf-2 significantly increased the neural excitability and the levels of IL-1β, IL-6, IL-10, TGF-β and TNF-α in Fer-1-treated SAH rats. Taken together, inhibiting the Nrf-2 induces early brain injury, brain edema and the inflammatory response with increasing of neural excitability in Fer-1-treated SAH rats. These results have indicated that inhibiting ferroptosis, neuroinflammation and neural excitability attenuates early brain injury after SAH by regulating the Nrf-2.

## 1. Introduction

Subarachnoid hemorrhage (SAH) is a subtype of stroke and has been reported to be related to high rates of mortality and poor prognoses (Calviere et al., 2019). Many studies have shown that ferroptosis plays a critical role in the development of early brain injury including neurological deficits, brain edema, and neuroinflammation after SAH (Cao et al., 2021). The early brain injury period was considered as the first 72 h after bleeding of SAH. Moreover, neuroinflammation contributes to neurological deficits and brain edema in early brain injury after SAH (Lai et al., 2020)., and inhibiting ferroptosis attenuates neurological deficits and neuroinflammation after SAH (Cao et al., 2021). However, the molecular mechanisms of the effects of inhibiting ferroptosis on neurological deficits, brain edema and neuroinflammation in the early brain injury of SAH remain unclear.

Ferrostatin-1 is widely applied to inhibit ferroptosis in various models, and its effects on inhibiting ferroptosis are more effective than those of phenolic antioxidants (Liu et al., 2020). Cao *et al.* illustrated that inhibiting ferroptosis attenuated neuroinflammation and neurological deficits without exploring the molecular mechanism (Cao et al., 2021). Thus, this study aims to explore the mechanisms of ferroptosis and neuroinflammation in early brain injury after SAH.

Nuclear factor E2-related factor (Nrf-2)/heme oxygenase 1 (Nrf2/HO-1) is a protein complex that is expressed in all cells of the animal and human bodies (Jin et al., 2022; Zhang et al., 2020). Nrf-2/HO-1 is involved in ferroptosis inhibition after intervertebral disc degeneration (IVDD) (Shao et al., 2022). Synergistic Nrf-2 pathways, including the Nrf-2/HO-1 pathway, Nrf-2/high mobility group box-1 (HMGB1) pathway and Nrf-2/HMGB1/toll-like receptor 4 (TLR4) pathway, exert neuroprotective effects in various rat models (Ali et al., 2021). The Nrf-2/HMGB1 pathway plays an important therapeutic role in protecting against myocardial ischemia and reperfusion injury by reducing the infarct size (Wang et al., 2014). Thus, we suspected that the Nrf-2/HMGB1/TLR4 signaling pathway can be a potential target to explore the detailed molecular mechanisms in early brain injury after SAH. However, it is still unknown whether the Nrf-2/HMGB1/TLR4

* Corresponding author.
*E-mail address:* doctor_duanzj@163.com (C. Duan).

https://doi.org/10.1016/j.brainresbull.2024.110877
Received 8 November 2023; Received in revised form 12 December 2023; Accepted 8 January 2024
Available online 11 January 2024

signaling pathway can regulate ferroptosis, neural excitability, neuroinflammation and brain edema in early brain injury after SAH.

This study aimed to explore the role of the Nrf-2/HMGB1/TLR4 signaling pathway in the early brain injury process of ferroptosis, neuroinflammation and excitability of hippocampal neurons after SAH. Therefore, our findings might provide a new molecular mechanism for the comprehensive treatment of early brain injury after SAH.

## 2. Materials and methods

### 2.1. Experimental animals, subarachnoid hemorrhage models and drug treatment

Adult male Sprague-Dawley (SD) rats (2 months old) were purchased from Guangdong Provincial Medical Experimental Animal Center. All animal studies were carried out according to protocols approved by the Laboratory Animal Ethics Committee of Southern Medical University (permit number: LAEC-2020–142.).

The subarachnoid hemorrhage (SAH) rat model was generated according to a previous study (Cao et al., 2021). Briefly, the rats were anesthetized with 1.5% isoflurane, and a 5–0 monofilament was inserted to the internal carotid artery and the bifurcation of the anterior and middle cerebral arteries via the left external carotid artery. Ferrostatin-1 (Fer-1, HY-100579, MedChemExpress) was dissolved in a working solution containing 10% DMSO, 40% PEG300, 5% Tween-80% and 45% saline by intraperitoneal injection (i.p.) 30 min after surgery. For the vehicle, the working solution was applied to SAH rats 30 min after surgery.

### 2.2. Measurement of subarachnoid hemorrhage grade and neurological score

The damage of the surgery was blindly measured at 6 h, 12 h, 24 h, 48 h and 72 h after SAH according to a previously reported SAH grading system. Briefly, the rats were anesthetized with 1.5% isoflurane, and the brain basal cistern was cut into six equal slices, each sample was scored from 0 to 3 and determined by presenting blood clotting. The SHA grades were the results from the sum scores of the six parts. Neurological function was measured by using the modified Garcia test (Garcia et al., 1995).

### 2.3. Brain water content

The rats were anesthetized with 1.5% isoflurane and then sacrificed after measuring neurological score. The rat brain was quickly removed after decapitation, and the brain was weighed immediately to measure its wet weight (WW). Then, the brains were dried at 105 ℃ for 72 h, and their dry weight (DW) was determined. The brain water content was calculated by the following formula: brain water content = [(WW-DW)/WW] × 100%.

### 2.4. Electrophysiology

The rats were anesthetized with 1.5% isoflurane and then sacrificed after measuring neurological score, and coronal hippocampal slices were collected by using a vibratome slicer (VT1200S; Leica). The electrophysiology experiments of coronal hippocampal slices in rat SAH were performed according to a previous study (Wang et al., 2023). To measure the excitatory spontaneous synaptic transmission and intrinsic excitability of pyramidal cells (PCs) in SAH rats, whole-cell patch clamp including current-clamp and voltage recordings were applied in this study. The coronal hippocampal slices were incubated with an oxygenated recording solution containing 125 mM NaCl, 2.5 mM KCl, 2 mM $CaCl_2$, 1 mM $MgCl_2$,1.25 mM $NaH_2PO_4$, 26 mM $NaHCO_3$, 25 mM D-glucose,1.3 mM sodium ascorbate, and 3.0 mM sodium pyruvate (pH 7.4) for 30 min. The brain slices were viewed by an upright microscope with a 40X water-immersion objective. To measure the neuronal excitability of PCs, APs were recorded by injecting a series of depolarizing currents (from 0 pA to 200 pA at a step of 10 pA) under the current-clamp model by holding resting membrane potential (RMP) at − 70 mV. And spontaneous excitatory postsynaptic currents (sEPSCs) were measured by holding the membrane potential at − 70 mV under the voltage recordings.

### 2.5. Measurement of $Fe^{3+}$ and $Fe^{2+}$ contents

The rats were anesthetized with 1.5% isoflurane and then sacrificed after measuring neurological score. The rat brain was quickly removed after decapitation. All the brains were ground with a glass mortar, and the lysate was diluted to 1/10 of the primary concentration by using PBS. The contents of $Fe^{3+}$ and $Fe^{2+}$ in the rat brain were measured by using an iron colorimetric assay kit (E-BC-K139-S, Elabscience, Wuhan, China) and ferrous iron colorimetric assay kit (E-BC-K773-M, Elabscience, Wuhan, China) according to the manufacturer's instructions. Rat brain was lysed with PBS and loaded with 1 μmol/1 calcein-AM for 30 min at 37 ℃. The calcein of the uncomplexed irons were measured by using a fluorescence microscope (Zeiss microscope) with quantify the fluorescence values.

### 2.6. Measurement of ROS

The rats were anesthetized with 1.5% isoflurane and then sacrificed after measuring neurological score. The rat brain was quickly removed after decapitation. All the brains were ground with a glass mortar and lysed with PBS buffer. The Dichloro-dihydro-fluorescein diacetate (DCFH-DA)-based reactive oxygen species (ROS) method was applied to explore the relative ROS level in the rat brain (Sun et al., 2021). A DCFH-DA solution was prepared with a centration of 10 mM in DMSO. All the brains were ground with a glass mortar, and the lysate was diluted to 1/10 of the primary concentration by using PBS.

### 2.7. Measurement of MDA and GSH-PX

The levels of malondialdehyde (MDA) and glutathione peroxidase (GSH-PX) were measured according to a previous study (Jin et al., 2022). The rat brains were harvested and diluted with PBS and applied to the MDA (ab118970, Abcam) and GSH-PX ELISA kits (ab239727, Abcam) according to the manufacturer's instructions.

### 2.8. Western blotting

Western blotting was performed according to previous study (Wang et al., 2023). The rats were anesthetized with 1.5% isoflurane and then sacrificed after measuring neurological score. The rat brain was quickly removed after decapitation. All the brains were ground with a glass mortar and lysed with RIPA buffer (Sigma Chemical Co., St. Louis MO, USA) containing protease and phosphatase inhibitors, and the samples were centrifuged at 12,000 rpm for 20 min at 4 ℃. The denatured samples with loading buffer at the temperature of 90–100 ℃ were separated on 10% SDS-PAGE gels. Proteins from the SDS-PAGE gels were transferred to a polyvinylidene difluoride (PVDF) membranes and blocked with 3% bovine serum albumin (BSA), and incubated with the following primary antibodies: HO-1 (diluted 1:1000; 43966, Cell Signaling Technology), Nrf-2 (diluted 1:1000; 20733 S, Cell Signaling Technology), TLR4 (diluted 1:1000; ab22048, Abcam), HMGB1 (diluted 1:1000; 6893 S, Cell Signaling Technology) and β-actin (diluted 1:1000; 3700 T, Cell Signaling Technology) were applied in this study. Then, the PVDF membranes were incubated with HRP-conjugated goat anti-rabbit or rat IgG (diluted 1:5000, Cell Signaling Technology) at room temperature for 1 h. The target proteins were revealed by using the Image Quant™ RT ECL System (GE Healthcare) and analyzed by using ImageJ software (ImageJ 1.5, National Institutes of Health, Bethesda, MD,

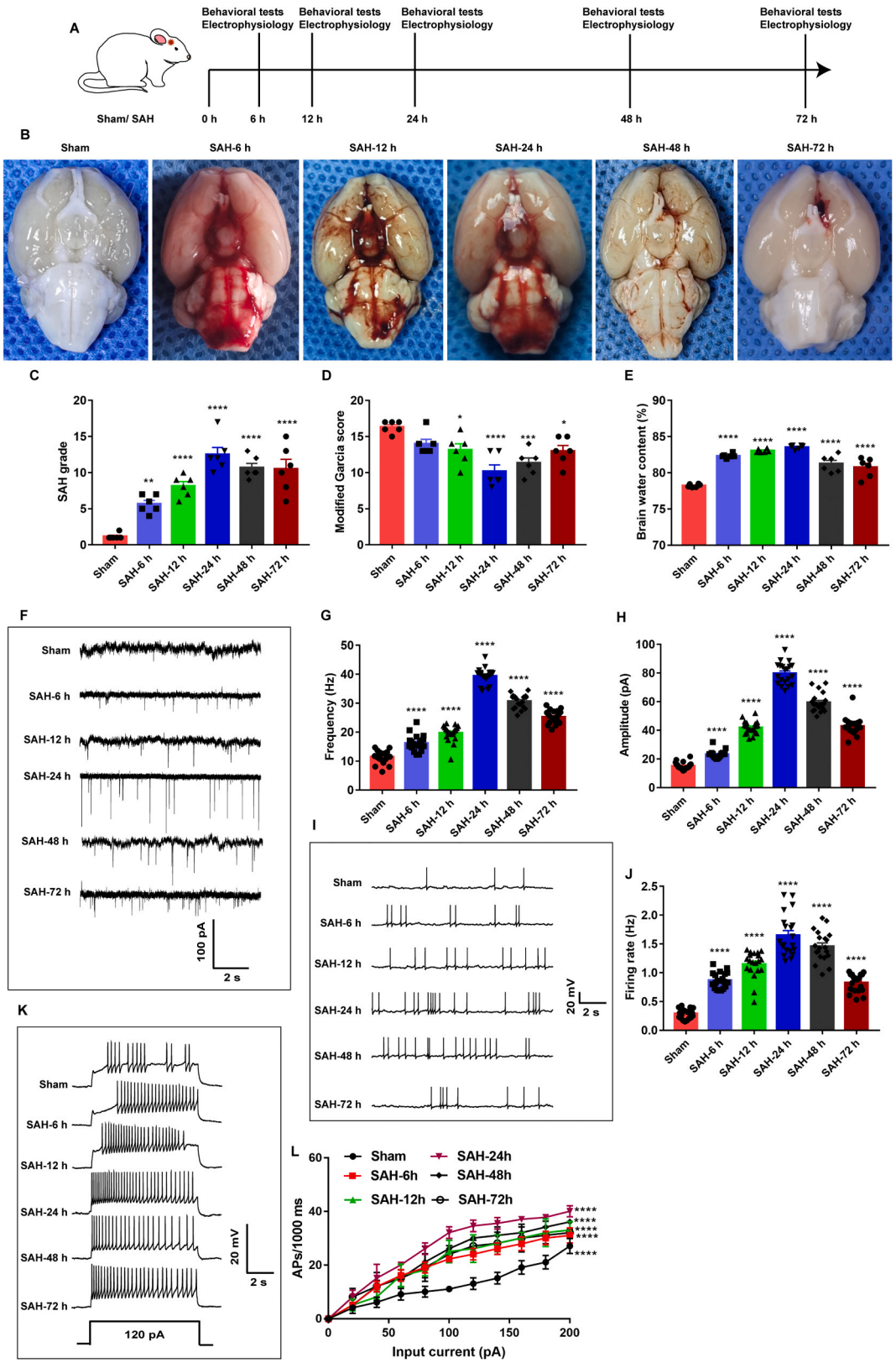


**Fig. 1.** SAH induced neurological deficits, brain edema and neural excitability in rats. (A) Experimental design and animal groups. (B) Typical photos of the brain from the Sham and SAH groups. (C) SAH grades for each group. (D) The modified Garcia score for each group. (E) Quantification of brain water content in each group. n = 6 mice for each group. (F) Representative current trace of sEPSCs of PCs in all six groups was recorded. Frequency (G) and amplitude (H) of sEPSCs were measured in all six groups. (I) Representative traces of spontaneous APs were presented. (J) Mean firing rate of spontaneous APs were calculated. (K) Representative traces of evoked APs of PCs were presented. (L) Number of evoked APs against the injected current in PCs were measured in all six groups. Data shown are means ± SEMs, n = 20 cells for each group. $^{*}P < 0.05$, $^{**}P < 0.01$, $^{***}P < 0.001$ and $^{****}P < 0.0001$ vs. sham. 2ANOVA with Tukey test was applied in this section.

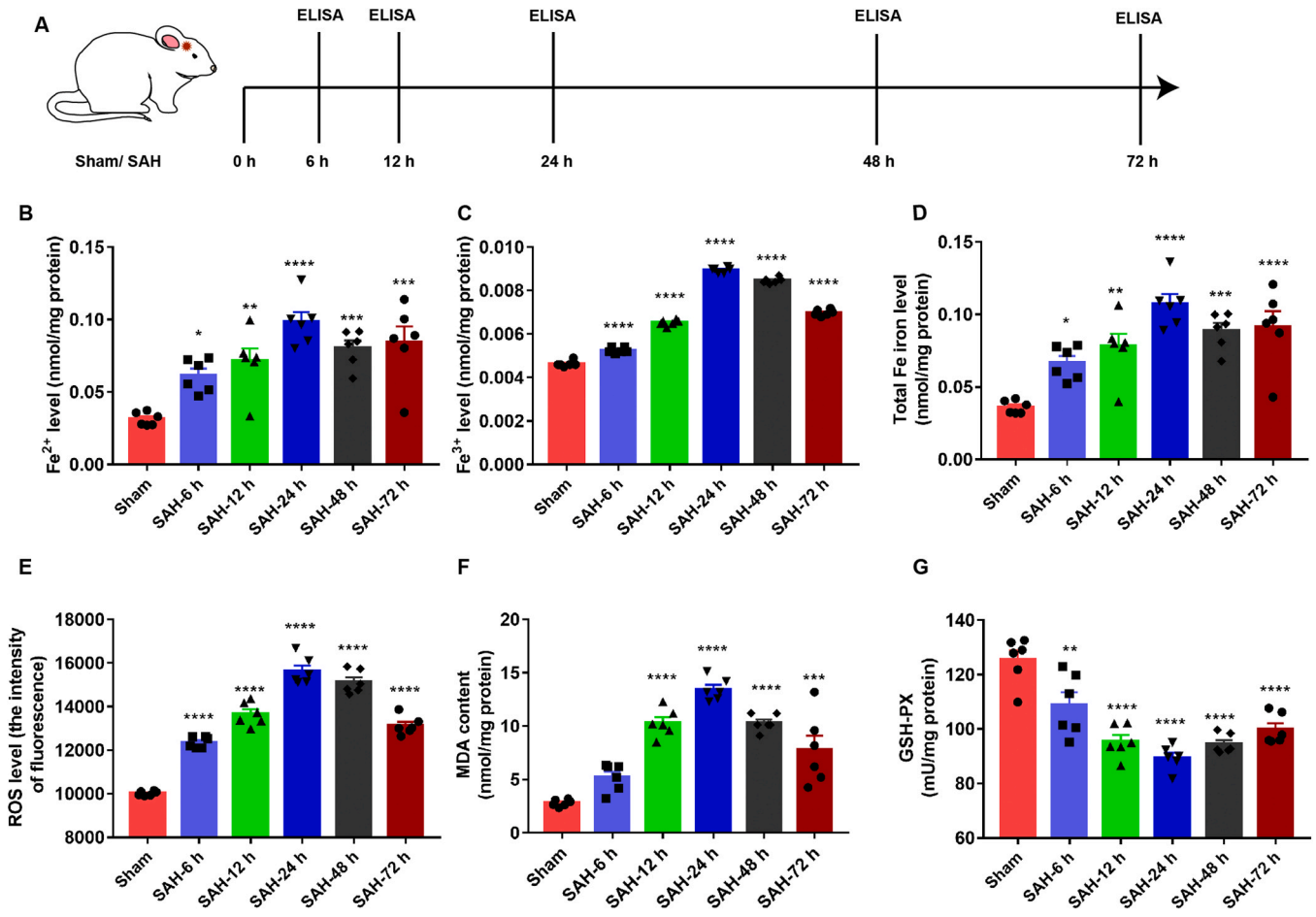


**Fig. 2.** SAH induced ferroptosis in rats. (A) Experimental design and animal groups. (B) $Fe^{2+}$ content in each group. (C) $Fe^{3+}$ content in each group. (D) Total Fe iron content in each group. (E) ROS level in each group. (F) MDA content in each group. (G) GSH-PX content in each group. Data shown are means ± SEMs (n = 6), ($^{*}p < 0.05$, $^{**}p < 0.01$, $^{***}p < 0.001$ and $^{****}p < 0.0001$ vs. sham). 2ANOVA with Tukey test was applied in this section.

United States).

### 2.9. Hematoxylin and eosin (H&E) staining

The brain samples were fixed with 4% paraformaldehyde and embedded in paraffin and were cut into 5 μm-thick sections. Paraffin-embedded rat right brains were stained with hematoxylin and eosin (H&E). The results of H&E staining were visualized using an optical microscope equipped with a charge-coupled device camera (Pulnix, Sunnyvale, CA, USA).

### 2.10. Transmission electron microscopy

The ultrastructure of mitochondria in the rat brain was observed by using transmission electron microscopy (TEM). Briefly, brains were collected and fixed in 2.5% glutaraldehyde for 2 h at 4 °C. Then, all the samples were transferred to 1% osmium tetroxide for 1 h at 4 °C. Then, the samples were dehydrated and embedded in epoxy resin. All the samples were sliced by using an ultramicrotome (RMC/MTX; Elexience). Ultrathin sections of 60–80 nm were mounted on copper grids and then applied to a Philips CM100 transmission electron microscope equipped with a TENGRA 2.3 K × 2.3 K TEM camera.

### 2.11. Cytokine assays

ELISA kits for rat cytokines, including IL-1β (900-M91, Camarillo, CA, USA), IL-6 (BMS625, Camarillo, CA, USA), IL-10 (BMS629, Camarillo, CA, USA), TGF-β (BMS623, Camarillo, CA, USA) and TNF-α (KRC3011, Camarillo, CA, USA), were purchased from BioSource International. All cytokine assays were performed according to the manufacturer's instructions.

### 2.12. Immunohistochemical staining

The brain samples were fixed with 4% paraformaldehyde and embedded in paraffin and were cut into 5 μm-thick sections. Paraffin-embedded rat right brains were stained with IHC. IHC was applied to explore the expression and distribution of Iba1, HO-1, Nrf-2, TLR4 and HMGB1 in the ipsilateral cortex after SAH. All slices were incubated overnight with the following primary antibody: anti-Iba1 (diluted 1:200, 17198 T, Cell Signaling Technology) Then, all slices were washed with PBS 3 times and incubated with biotinylated goat anti-rabbit IgG (H+L) (diluted 1:100; ab64256, Abcam). Then, enzyme-labeled streptavidin was applied and incubated according to the manufacturer's protocol.

### 2.13. Intracerebroventricular injections of siRNA

*Nrf2* siRNA with the sense strand 5′- GTC TTC AGC ATG TTA CGT GAT GAG GAT GG-3′ and its control siRNA were synthesized by Sangon Biotech (Shanghai, China) and dissolved in RNase-free resuspension buffer at a concentration of 500 pmol/μL. Intracerebroventricular (i.c.v) injection was applied to administer siRNAs to the right ventricle according to a previous study (Wilmes et al., 2022).

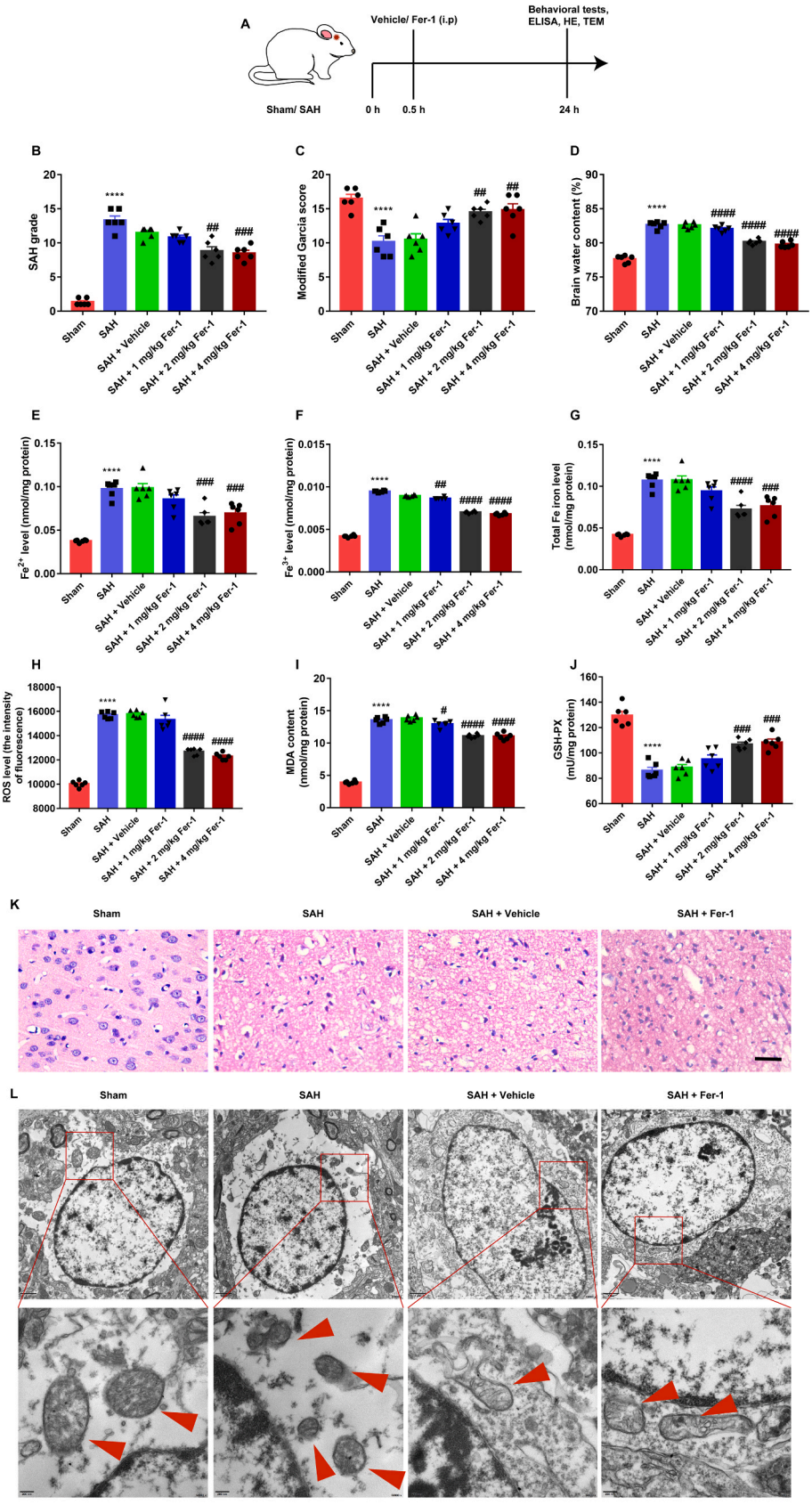


*(caption on next page)*

**Fig. 3.** Neurological deficits, brain edema and ferroptosis were attenuated by ferrostatin-1 in SAH rats. (A) Experimental design and animal groups. (B) SAH grades for each group. (C) The modified Garcia score for each group. (D) Quantification of brain water content in each group. (E) $Fe^{2+}$ content in each group. (F) $Fe^{3+}$ content in each group. (G) Total Fe iron content in each group. (H) ROS level in each group. (I) MDA content in each group. (J) GSH-PX content in each group. Data shown are means ± SEMs (n = 6), ($^{***}P < 0.001$ and $^{****}P < 0.0001$ vs. sham, $^{\#\#}P < 0.01$, $^{\#\#\#}P < 0.001$ and $^{\#\#\#\#}P < 0.0001$ vs. SAH). (K) Typical photomicrographs of H&E staining (magnification = ×400, scale bar = 50 μm, n = 3 per group). (L) Typical TEM photomicrographs. magnification = ×8000–50000, scale bar = 200 nm-2 μm, n = 3 per group.

### 2.14. Statistical analysis

GraphPad Prism (Version 7.0, San Diego, CA) was applied to analyze the data in this study. All the data were presented as the mean ± standard error (SEM). The statistical significance of differences between two groups was assessed by using Student's *t* test, and the statistical significance of multiple groups was calculated by using two-way analysis of variance (2ANOVA) followed by Tukey multiple comparisons test, as shown in the results. $P < 0.05$ was considered to indicate statistical significance.

## 3. Results

### 3.1. SAH induced neurological deficit and brain edema

The number of rats used in this study was 394, including the rats that died or were excluded from each group. Behavioral tests were performed 6 h, 12 h, 24 h, 48 h and 72 h after SAH (Fig. 1A). Typical photos of the brains from the Sham and SAH groups are shown in Fig. 1B. Our results showed that the SAH grade score was significantly increased in SAH group rats at different time points compared to the sham group, and it peaked at 24 h after SAH (Fig. 1C). The modified Garcia test showed that the SAH rats exerted a significant neurological deficit compared to the sham group, and the modified Garcia score was lowest at 24 h after SAH (Fig. 1D). The brain water content was significantly increased in SAH group rats compared to the sham group and peaked at 24 h after SAH (Fig. 1E).

### 3.2. SAH increased spontaneous synaptic transmission and intrinsic excitability of CA1 pyramidal cells (PCs)

Our results indicate that frequency (Fig. 1F, G) and amplitude (Fig. 1F, H) of spontaneous excitatory postsynaptic currents (sEPSCs) were unregulated in SAH group compared to sham group and peaked at 24 h after SAH. Moreover, the number of spontaneous action potentials (APs) (Fig. 1I, J) and current-evoked APs (Fig. 1K, L) were increased in

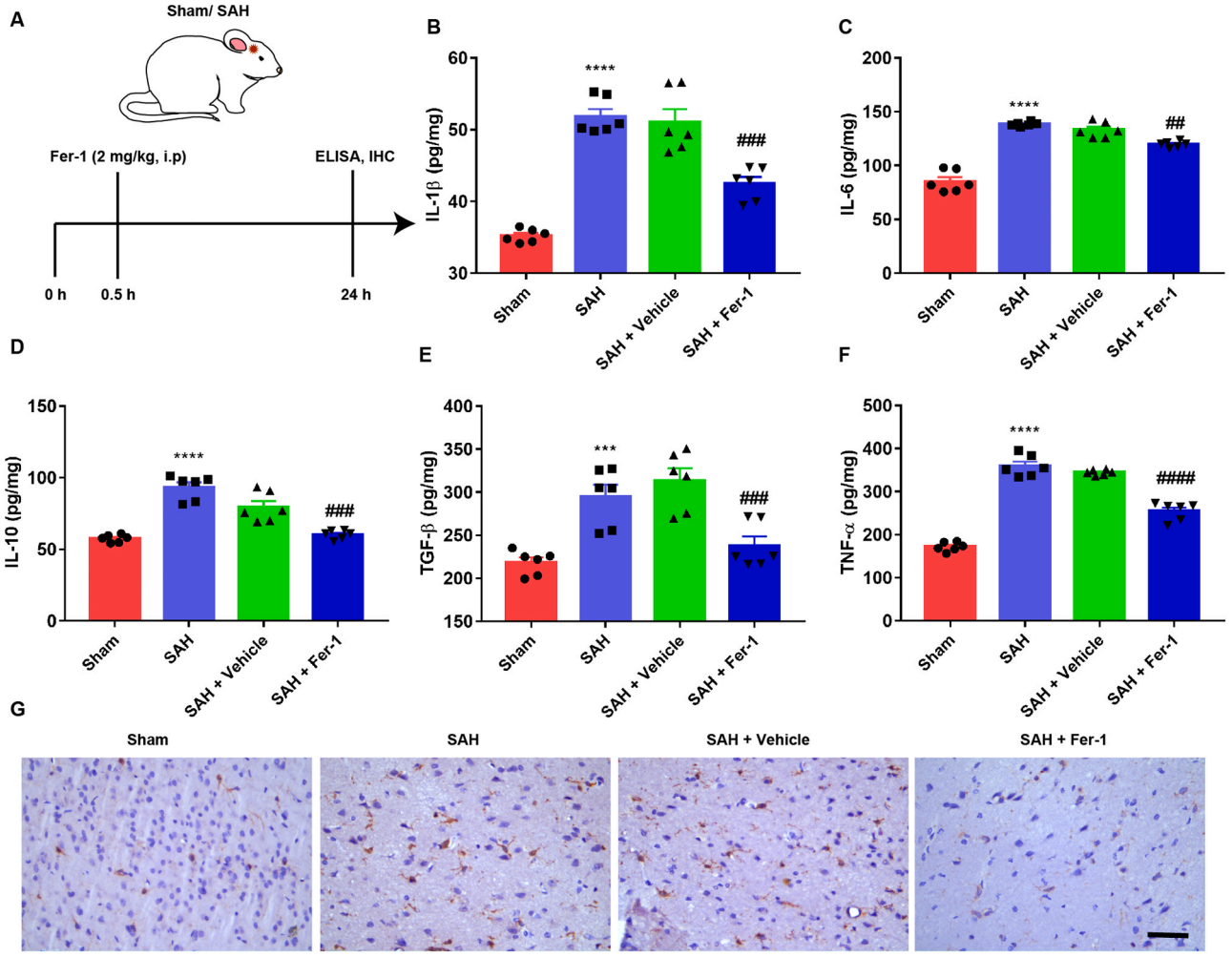


**Fig. 4.** Ferrostatin-1 suppressed the inflammatory response in SAH rats. (A) Experimental design and animal groups. Quantitative analysis of IL-1β (B), IL-6 (C), IL-10 (D), TGF-β (E) and TNF-α (F) by ELISA. Data shown are means ± SEMs (n = 6), ($^{***}P < 0.001$ and $^{****}P < 0.0001$ vs. sham, $^{\#\#}P < 0.01$, $^{\#\#\#}P < 0.001$ and $^{\#\#\#\#}P < 0.0001$ vs. SAH). (G) Typical photomicrographs of Iba1 staining. Magnification = ×400, scale bar = 50 μm, n = 3 per group.

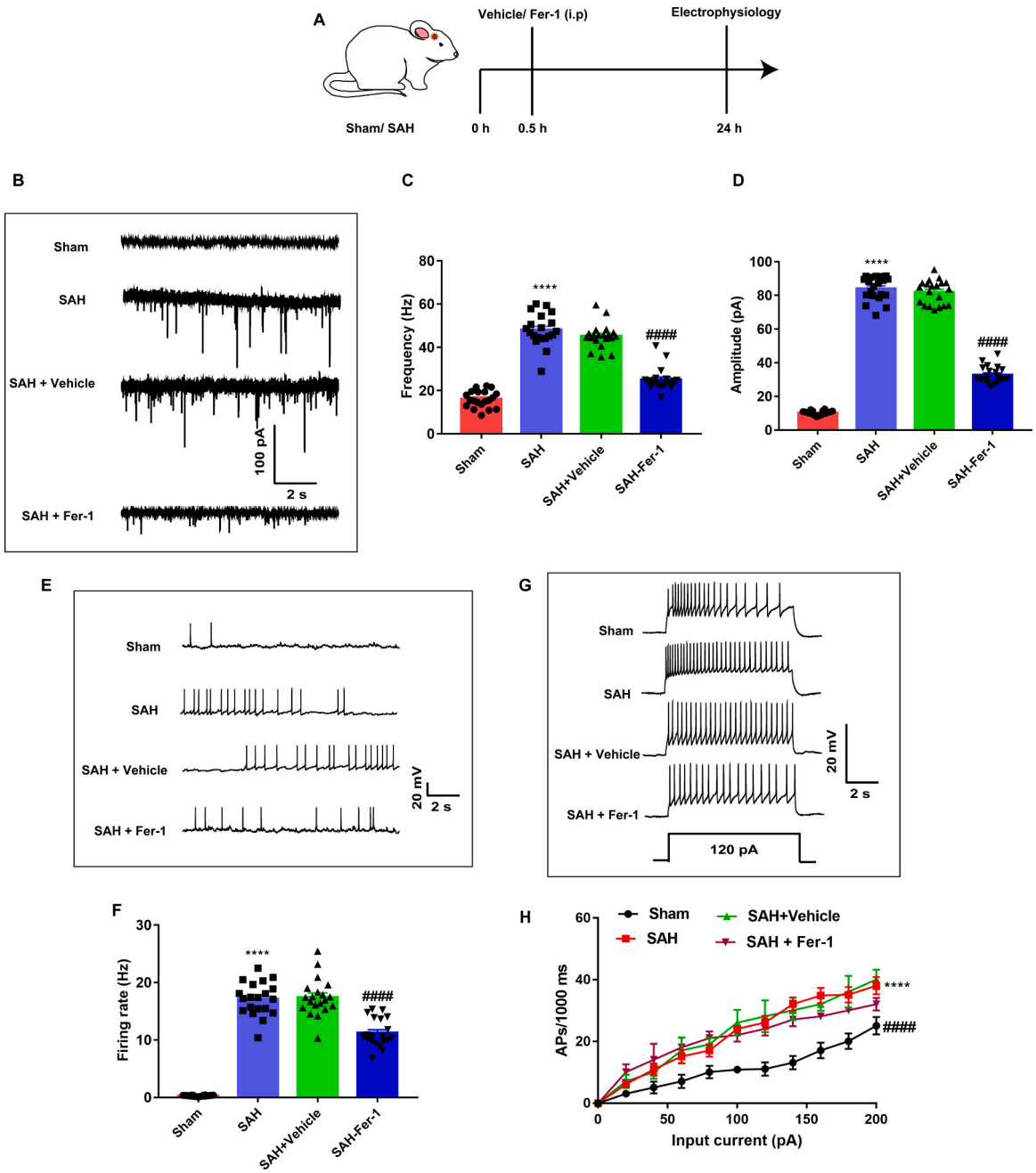


**Fig. 5.** Ferrostatin-1 decreased neural excitability in SAH rats. (A) Experimental design and animal groups. (B) Representative current traces of sEPSCs of PCs in all four groups were recorded. Frequency (C) and amplitude (D) of sEPSCs were measured in all four groups. (E) Representative traces of spontaneous APs were presented. (F) Mean firing rate of spontaneous APs were calculated. (G) Representative traces of evoked APs of PCs in all four groups was presented. (H) Number of evoked APs against the injected current in PCs were measured in all four groups. Data shown are means ± SEMs, n = 20 cells for each group. $^{****}P < 0.0001$ vs. sham, $^{\#\#\#\#}P < 0.0001$ vs. SAH+Vehicle, 2ANOVA with Tukey test was applied in this section. SAH, subarachnoid hemorrhage.

SAH group compared to sham group and peaked at 24 h after SAH.

### 3.3. SAH induced ferroptosis in rats

ELISA was performed 6 h, 12 h, 24 h, 48 h and 72 h after SAH (Fig. 2A), total Fe iron, $Fe^{2+}$ and $Fe^{3+}$, reactive oxygen species (ROS), malondialdehyde (MDA) and glutathione peroxidase (GSH-PX) levels were measured to explore the effects of SAH on ferroptosis in the brain. The results showed that the brain $Fe^{2+}$ (Fig. 2B), $Fe^{3+}$ (Fig. 2C) and total Fe iron level (Fig. 2D) were significantly increased in SAH group rats at different time points compared to the sham group and peaked at 24 h after SAH. Moreover, the levels of ROS (Fig. 2E), MDA (Fig. 2F) and GSH-PX (Fig. 2G) were significantly increased in SAH group rats at different time points compared to the sham group and peaked at 24 h after SAH.

### 3.4. Neurological deficits, brain edema and ferroptosis were attenuated by ferrostatin-1 in SAH rats

To explore the role of ferroptosis in SAH rats, three doses (1, 2 and 4 mg/kg) of ferrostatin-1 (Fer-1) were applied at 0.5 h after SAH, and ELISA and behavioral tests were performed at 24 h after SAH (Fig. 3A). Our results showed that the SAH grade score (Fig. 3B) and brain water content (Fig. 3D) were significantly decreased in the Fer-1-treated

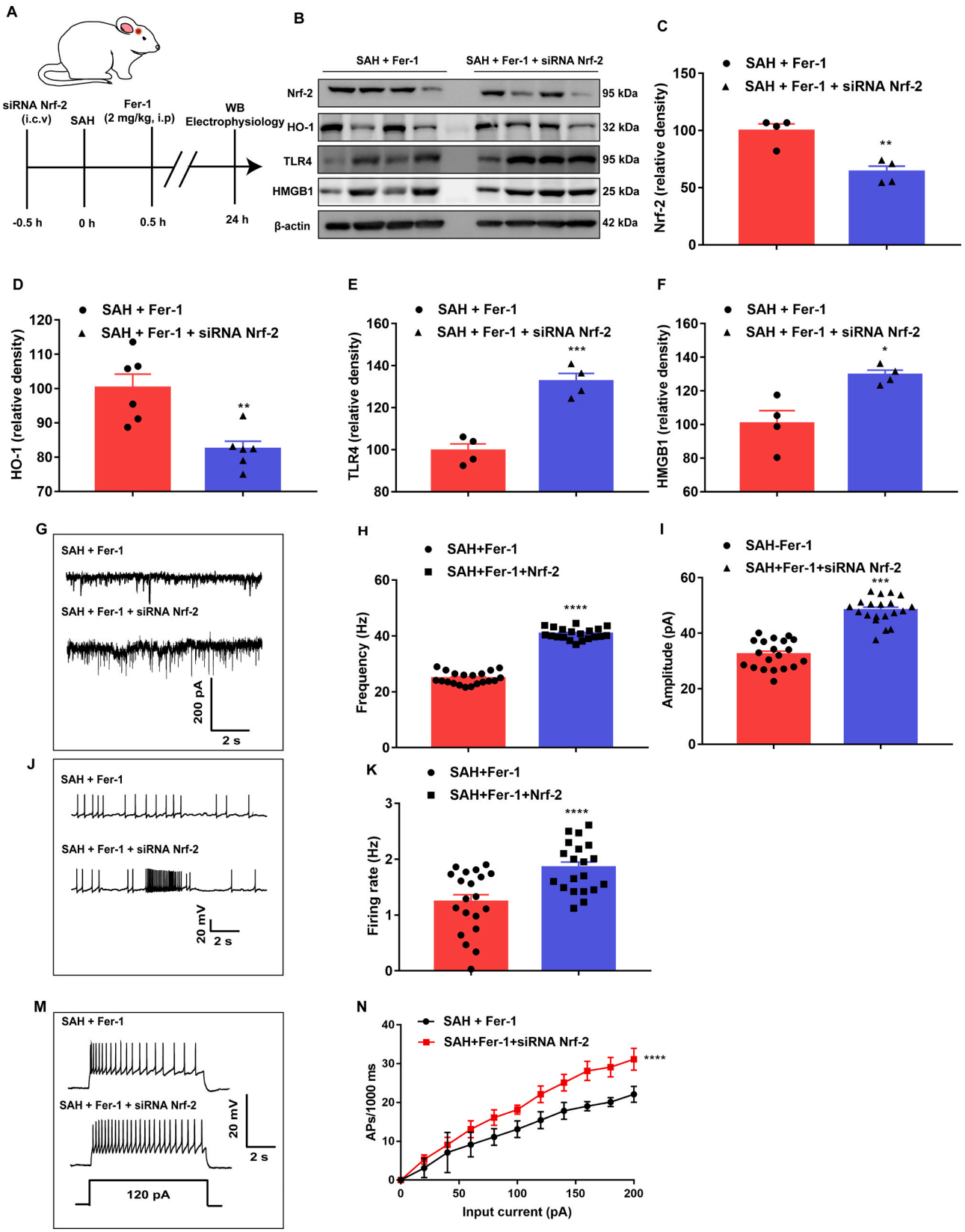


**Fig. 6.** Inhibiting the Nrf-2 increases neural excitability in SAH rats. (A) Experimental design and animal groups. (B) Western blotting analysis of the indicated proteins was performed, and β-actin was used as the loading control. Nrf-2 (C), HO-1 (D), TLR4 (E) and HMGB1 (F) were measured. Data shown are means ± SEMs (n = 4), ($^{*}P < 0.05$, $^{**}P < 0.01$ and $^{***}P < 0.001$ vs. SAH + Fer-1). (G) Representative current trace of sEPSCs of PCs in the two groups was recorded. Frequency (H) and amplitude (I) of sEPSCs were measured in two groups. (J) Representative traces of spontaneous APs were presented. (K) Mean firing rate of spontaneous APs were calculated. (M) Representative traces of evoked APs of PCs in two groups was presented. (N) Number of evoked APs against the injected current in PCs were measured in two groups. $^{****}P < 0.0001$ vs. sham, n = 20 cells for each group, 2ANOVA with Tukey test was applied in this section.

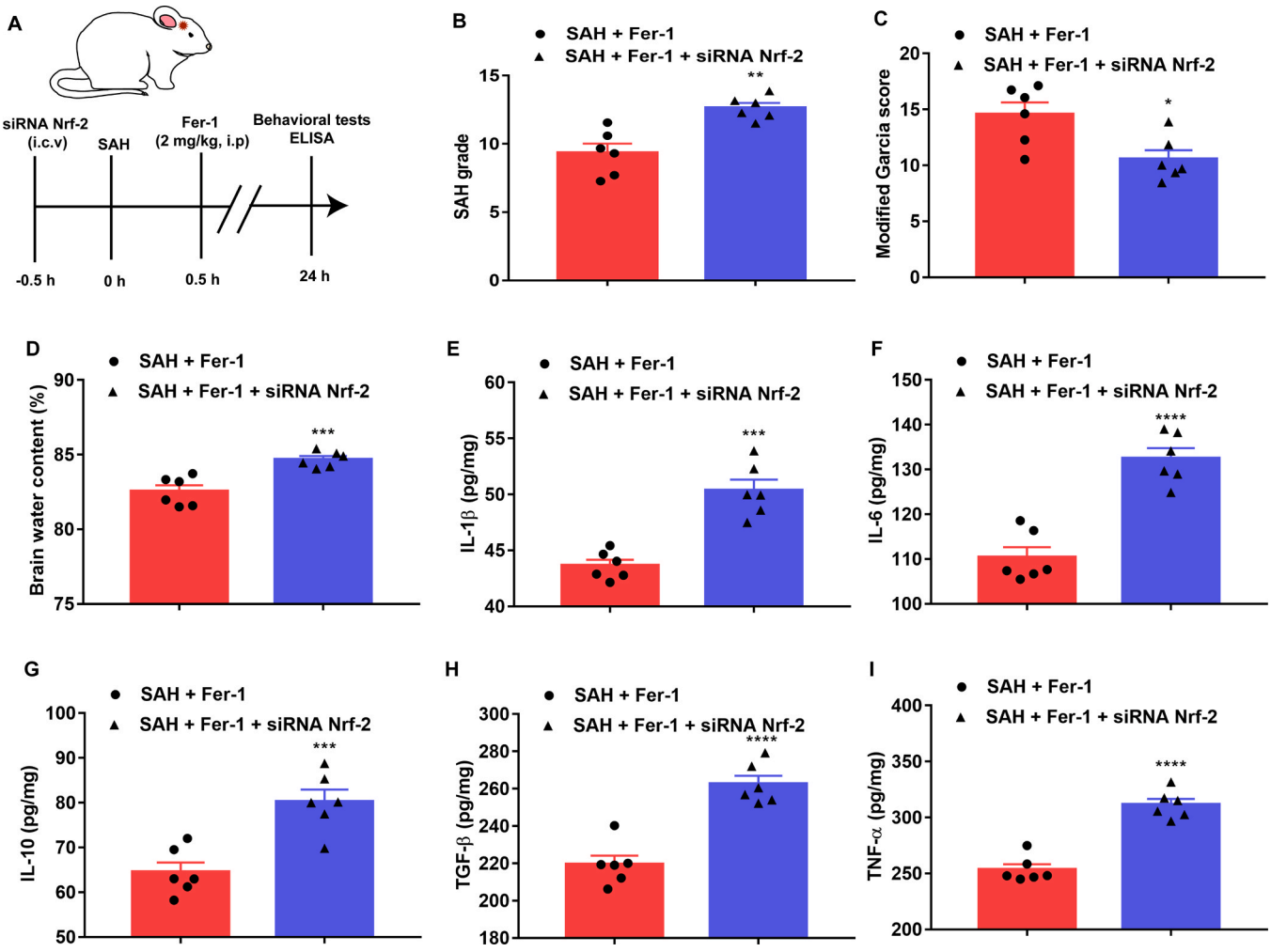


**Fig. 7.** Inhibiting the Nrf-2/HMGB1/TLR4 signaling pathway induces early brain injury, brain edema and inflammatory response in SAH rats. (A) Experimental design and animal groups. (B) SAH grades for each group. (C) The modified Garcia score for each group. (D) Quantification of brain water content in each group. (n = 6). $^{*}P < 0.05$, $^{**}p < 0.01$, $^{***}P < 0.001$ and $^{****}P < 0.0001$ vs. sham. Quantitative analysis of IL-1β (E), IL-6 (F), IL-10 (G), TGF-β (H) and TNF-α (I) by ELISA. Data shown are means ± SEMs (n = 6). $^{***}P < 0.001$ and $^{****}P < 0.0001$ vs. sham.

groups at doses of 2 mg/kg or 4 mg/kg compared to the SAH group. Meanwhile, the modified Garcia score was significantly increased in the Fer-1-treated groups at doses of 2 mg/kg or 4 mg/kg compared to the SAH group (Fig. 3C).

### 3.5. Ferrostatin-1 suppressed ferroptosis in SAH rats

Meanwhile, we found that the brain $Fe^{2+}$ (Fig. 3E), $Fe^{3+}$ (Fig. 3F) and total Fe iron (Fig. 3G) levels were significantly decreased in the ferrostatin-1 treatment group compared to the SAH group. The ROS level (Fig. 3H) and MDA (Fig. 3I) content were significantly decreased in the Fer-1-treated groups at doses of 2 mg/kg or 4 mg/kg compared to the SAH group. Moreover, the content of GSH-PX was significantly increased in the Fer-1-treated groups at doses of 2 mg/kg or 4 mg/kg compared to the SAH group (Fig. 3J). The results of H&E staining showed that cavities and tissue damage were increased in SAH group rats compared to sham group rats, and 2 mg/kg ferrostatin-1 treatment decreased the cavities and tissue damage after SAH treatment (Fig. 3K). Furthermore, we found that a reduction in volume and ruptured mitochondria occurred in SAH group rats compared to sham group rats, and 2 mg/kg ferrostatin-1 treatment reversed the reduction in volume and ruptured mitochondria in SAH group rats (Fig. 3L).

### 3.6. Ferrostatin-1 suppressed the inflammatory response in SAH rats

Ferrostatin-1 (2 mg/kg) was applied at 0.5 h after SAH, and ELISA and immunohistochemical staining (IHC) were performed 24 h after SAH (Fig. 4A). The results showed that the levels of IL-1β (Fig. 4B), IL-6 (Fig. 4C), IL-10 (Fig. 4D), TGF-β (Fig. 4E) and TNF-α (Fig. 4F) in SAH group rats were significantly increased compared to those in sham group rats. Moreover, 2 mg/kg ferrostatin-1 treatment significantly decreased the expression of IL-1β (Fig. 4B), IL-6 (Fig. 4C), IL-10 (Fig. 4D), TGF-β (Fig. 4E) and TNF-α (Fig. 4D). Moreover, the IHC results showed that microglia were activated in the brains of SAH group rats, and 2 mg/kg ferrostatin-1 treatment inhibited the activity of microglia in SAH rats (Fig. 4G).

### 3.7. Ferrostatin-1 suppressed excitatory spontaneous synaptic transmission and intrinsic excitability of PCs in SAH rats

Here, 2 mg/kg of ferrostatin-1 was applied at 0.5 h after SAH and electrophysiology experiments were performed at 24 h after SAH to explore the role of excitatory spontaneous synaptic transmission and intrinsic excitability of PCs in SAH rats (Fig. 5A). Our results have shown that frequency (Fig. 5B, C) and amplitude (Fig. 5B, D) of sEPSCs in PCs were significant increased in SAH+Fer-1 group compared to SAH+Vehicle group. the number of spontaneous APs (Fig. 5E, F) and

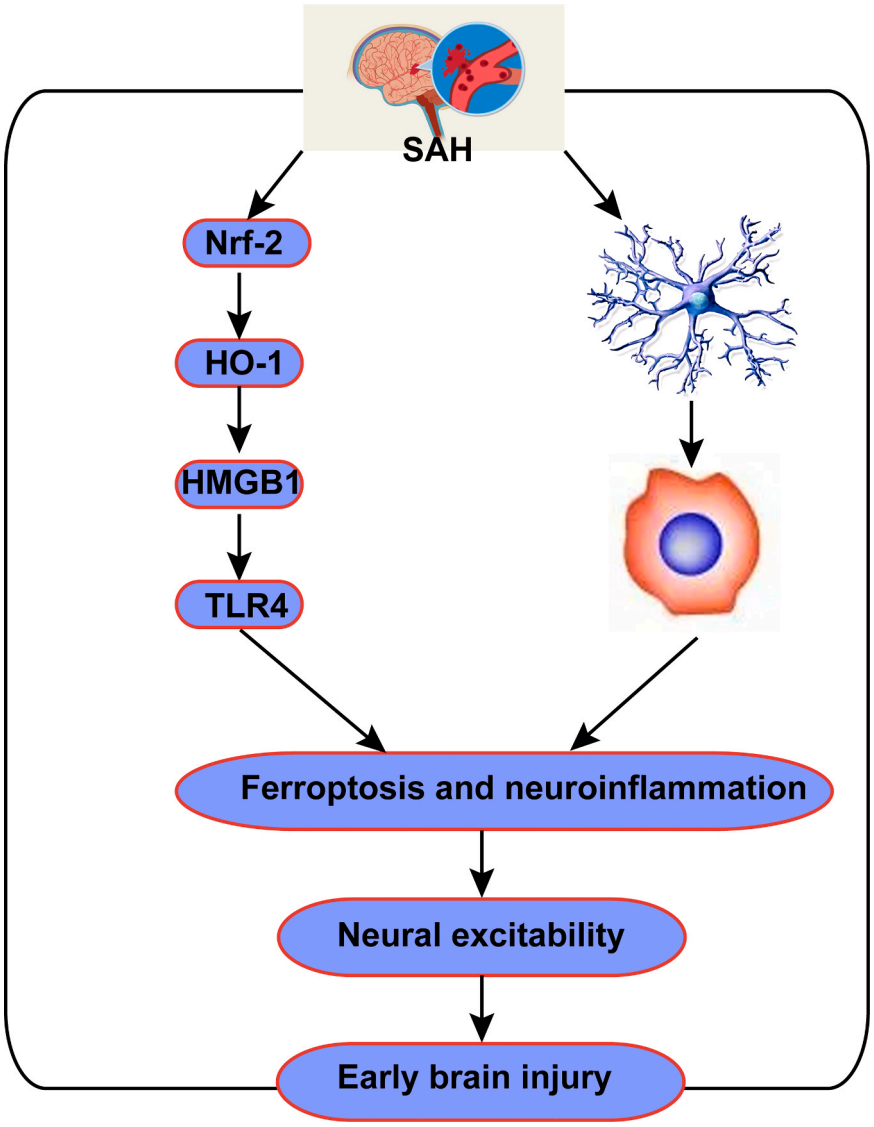


**Fig. 8.** Inhibiting ferroptosis, neuroinflammation and neural excitability attenuates early brain injury after SAH by regulating the Nrf-2. Our results indicated that SAH induced neurological deficits, brain edema, ferroptosis, neuroinflammation and neural excitability in rats. Ferrostatin-1 treatment significantly decreased the expression and distribution of IL-1β, IL-6, IL-10, TGF-β and TNF-α. Inhibiting ferroptosis by ferrostatin-1 can attenuate neural excitability, neurological deficits, brain edema and neuroinflammation in SAH rats. Inhibiting the expression of Nrf-2 significantly increased the neural excitability and the levels of IL-1β, IL-6, IL-10, TGF-β and TNF-α in Fer-1-treated SAH rats. Taken together, our results have indicated that inhibiting ferroptosis, neuroinflammation and neural excitability attenuates early brain injury after SAH by regulating the Nrf-2.

current-evoked APs (Fig. 5G, H) were increased in SAH+Fer-1 group compared to SAH+Vehicle group.

### 3.8. Inhibiting the Nrf-2 induces early brain injury in SAH rats

In this study, the expression of Nrf-2 was modulated by intracerebroventricular (i.c.v) injections of *Nrf-2* siRNA 0.5 h before SAH (Fig. 6A, Fig. 7A). Fer-1 (2 mg/kg) was applied at 0.5 h after SAH, then WB, behavioral tests, and electrophysiology experiments were performed at 24 h after SAH (Figs. 6A, 7A). The results showed that i.c.v. injections of *Nrf-2* siRNA significantly decreased the protein expression of Nrf-2 (Fig. 6B, C) and HO-1 (Fig. 6B, D) and significantly increased the protein expression of TLR4 (Fig. 3B, E) and HMGB1 (Fig. 6B, F). Thus, i.c.v. injections of siRNA *Nrf-2* inhibited the Nrf-2/HMGB1/TLR4 signaling pathway in Fer-1-treated SAH rats. Furthermore, injections of *Nrf-2* siRNA significantly increased SAH grade (Fig. 7B) and brain water content (Fig. 7D) and decreased the modified Garcia score (Fig. 7C) in Fer-1-treated SAH rats.

### 3.9. Inhibiting the Nrf-2 increases excitatory spontaneous synaptic transmission and intrinsic excitability of PCs in SAH rats

Our results have shown that injections of *Nrf-2* siRNA significantly increased frequency (Fig. 6G, H) and amplitude (Fig. 6G, I) of sEPSCs in PCs in SAH+Fer-1 group. And the number of spontaneous APs (Fig. 6J, K) current-evoked APs (Fig. 6M, N) was significantly increased after treatment with *Nrf-2* siRNA. Taken together, our results have shown that inhibiting the Nrf-2/HMGB1/TLR4 signaling pathway increase neural excitability of PCs in Fer-1-treated SAH rats.

### 3.10. Inhibiting the Nrf-2 induces inflammatory response in SAH rats

Fer-1 (2 mg/kg) was applied at 0.5 h after SAH, then ELISA was performed at 24 h after SAH (Fig. 7A). In this study, we found that injections of siRNA *Nrf-2* significantly increased the levels of IL-1β (Fig. 7E), IL-6 (Fig. 7F), IL-10 (Fig. 7G), TGF-β (Fig. 7H) and TNF-α (Fig. 7I) in Fer-1-treated SAH rats.

## 4. Discussion

Recent studies have revealed the involvement of ferroptosis in various neurological conditions, specifically its connection to neurological deficits, brain edema, and neuroinflammation (Cao et al., 2021). Inhibiting ferroptosis has been shown to alleviate early brain injury by reducing lipid peroxidation (Li et al., 2021) and iron-dependent oxidative cell injury (Chen-Roetling et al., 2018). Our study conducted time-point experiments to establish a subarachnoid hemorrhage (SAH) rat model, focusing on early brain injury. We observed peak levels of neurological deficits, ferroptosis, brain edema, and neural excitability in CA1 pyramidal cells (PCs) at 24 h post-SAH. Consequently, we selected the SAH-24 h group for further exploration of ferroptosis's molecular mechanisms in SAH rats.

Nuclear factor E2-related factor (Nrf-2), a leucine zipper transcriptional activating factor in the cap-n-collar (CNC) family (Kim et al., 2013), plays a crucial role in protecting the hemorrhagic brain. It reduces lesion volume, neurologic deficits, brain edema, and reactive oxygen species (Chang et al., 2014). The Nrf-2/high mobility group box-1 (HMGB1) and Nrf-2/HMGB1/toll-like receptor 4 (TLR4) signaling pathways are implicated in neurodegeneration and cognitive deficits across various neurological disorders. This led us to hypothesize that the Nrf-2/HMGB1/TLR4 pathway might be key in the molecular mechanism of early brain injury in SAH rats. We inhibited this pathway using intracerebroventricular injections of Nrf-2 siRNA in the right lateral ventricle. Our results indicated that these injections significantly altered the protein expression associated with this pathway and worsened SAH severity and brain water content while reducing the modified Garcia score. This suggests that suppressing the Nrf-2/HMGB1/TLR4 pathway may worsen neurological deficits and brain edema. Furthermore, this inhibition noticeably increased the levels of various inflammatory markers in Fer-1-treated SAH rats.

In conclusion, our findings demonstrate that ferrostatin-1 effectively inhibits ferroptosis, which in turn reduces neurological deficits, brain edema, and neuroinflammation in early SAH brain injury. Conversely, inhibiting the Nrf-2/HMGB1/TLR4 pathway aggravates early brain injury, increases brain edema, and triggers an inflammatory response. These insights highlight the potential of targeting the Nrf-2/HMGB1/TLR4 pathway as a treatment strategy for early brain injury in SAH (Fig. 8).

Although our findings illustrated that inhibiting ferroptosis, neuroinflammation and neural excitability attenuates early brain injury after SAH by regulating the Nrf-2, there are still some challenges to be settled in our future study, such as 1) Nrf-2 gene knock mice should be applied to verify the role of Nrf-2 in the brain injury, brain edema of SAH rats, 2) try to explore the role of Nrf-2 IN regulating the neural excitability of PCs by using photogenetics and chemical genetics, 3) try to confirm these findings and explore the Nrf-2 for treating early brain injury with reducing brain edema and the inflammatory response in SAH.

## Funding

This project was supported by National Natural Science Foundation of China, Grant number: 81974178; Scientific Research Projects of Huaian Health Commission, Grant number: HAWJ202005; Science and Technology Development Fund of Nanjing Medical University, Grant number: NMUB2020148.

## CRediT authorship contribution statement

**Dazhao Fang**: Conceptualization, Methodology, Data curation, Writing – original draft. **Shenquan Guo**: Methodology, Data curation. **Boyang Wei**: Methodology, Data curation. **Wenchao Liu**: Software, Validation. **Guangxu Li**: Investigation, Data curation. **Xifeng Li**: Methodology. **Jiahui Liu**: Methodology, Data curation. **Lei Jin**: Methodology. **Chuanzhi Duan**: Investigation, Supervision, Writing – review &editing.

## Declaration of Competing Interest

All authors declare no conflict of interests.

## Data availability

No data was used for the research described in the article.

## References

Calviere, L., Viguier, A., Patsoura, S., Rousseau, V., Albucher, J.F., Planton, M., Pariente, J., Cognard, C., Olivot, J.M., Bonneville, F., Raposo, N., 2019. Risk of intracerebral hemorrhage and mortality after convexity subarachnoid hemorrhage in cerebral amyloid angiopathy. Stroke 50, 2562–2564. https://doi.org/10.1161/STROKEAHA.119.026244.

Cao, Y., Li, Y., He, C., Yan, F., Li, J.R., Xu, H.Z., Zhuang, J.F., Zhou, H., Peng, Y.C., Fu, X. J., Lu, X.Y., Yao, Y., Wei, Y.Y., Tong, Y., Zhou, Y.F., Wang, L., 2021. Selective ferroptosis inhibitor liproxstatin-1 attenuates neurological deficits and neuroinflammation after subarachnoid hemorrhage. Neurosci. Bull. 37, 535–549. https://doi.org/10.1007/s12264-020-00620-5.

Chang, C.F., Cho, S., Wang, J., 2014. (-)-Epicatechin protects hemorrhagic brain via synergistic Nrf2 pathways. Ann. Clin. Transl. Neurol. 1, 258–271. https://doi.org/10.1002/acn3.54.

Chen-Roetling, J., Ma, S.K., Cao, Y., Shah, A., Regan, R.F., 2018. Hemopexin increases the neurotoxicity of hemoglobin when haptoglobin is absent. J. Neurochem 145, 464–473. https://doi.org/10.1111/jnc.14328.

Garcia, J.H., Wagner, S., Liu, K.F., Hu, X.J., 1995. Neurological deficit and extent of neuronal necrosis attributable to middle cerebral artery occlusion in rats. Statistical validation. discussion 635 Stroke 26, 627–634. https://doi.org/10.1161/01.str.26.4.627.

Jin, L., Jin, F., Guo, S., Liu, W., Wei, B., Fan, H., Li, G., Zhang, X., Su, S., Li, R., Fang, D., Duan, C., Li, X., 2022. Metformin Inhibits NLR Family Pyrin Domain Containing 3 (NLRP)-Relevant Neuroinflammation via an Adenosine-5′-Monophosphate-Activated Protein Kinase (AMPK)-Dependent Pathway to Alleviate Early Brain Injury After Subarachnoid Hemorrhage in Mice. Front Pharm. 13, 796616 https://doi.org/10.3389/fphar.2022.796616.

Kim, J.H., Yu, S., Chen, J.D., Kong, A.N., 2013. The nuclear cofactor RAC3/AIB1/SRC-3 enhances Nrf2 signaling by interacting with transactivation domains. Oncogene 32, 514–527. https://doi.org/10.1038/onc.2012.59.

Lai, N., Wu, D., Liang, T., Pan, P., Yuan, G., Li, X., Li, H., Shen, H., Wang, Z., Chen, G., 2020. Systemic exosomal miR-193b-3p delivery attenuates neuroinflammation in early brain injury after subarachnoid hemorrhage in mice. J. Neuroinflamm. 17, 74 https://doi.org/10.1186/s12974-020-01745-0.

Li, Y., Liu, Y., Wu, P., Tian, Y., Liu, B., Wang, J., Bihl, J., Shi, H., 2021. Inhibition of ferroptosis alleviates early brain injury after subarachnoid hemorrhage in vitro and in vivo via reduction of lipid peroxidation. Cell Mol. Neurobiol. 41, 263–278. https://doi.org/10.1007/s10571-020-00850-1.

Liu, P., Feng, Y., Li, H., Chen, X., Wang, G., Xu, S., Li, Y., Zhao, L., 2020. Ferrostatin-1 alleviates lipopolysaccharide-induced acute lung injury via inhibiting ferroptosis. Cell Mol. Biol. Lett. 25 doi:10. 10.1186/s11658-020-00205-0.

Shao, Y., Sun, L., Yang, G., Wang, W., Liu, X., Du, T., Chen, F., Jing, X., Cui, X., 2022. Icariin protects vertebral endplate chondrocytes against apoptosis and degeneration via activating Nrf-2/HO-1 pathway. Front Pharm. 13, 937502 https://doi.org/10.3389/fphar.2022.937502.

Sun, K., Luo, J., Jing, X., Xiang, W., Guo, J., Yao, X., Liang, S., Guo, F., Xu, T., 2021. Hyperoside ameliorates the progression of osteoarthritis: An in vitro and in vivo study. Phytomedicine 80, 153387. https://doi.org/10.1016/j.phymed.2020.153387.

Wang, J., Hu, X., Jiang, H., 2014. Nrf-2-HO-1-HMGB1 axis: an important therapeutic approach for protection against myocardial ischemia and reperfusion injury. Int J. Cardiol. 172, 223–224. https://doi.org/10.1016/j.ijcard.2013.12.273.

Wang, W., Zhang, X., He, R., Li, S., Fang, D., Pang, C., 2023. Gamma frequency entrainment rescues cognitive impairment by decreasing postsynaptic transmission after traumatic brain injury. CNS Neurosci. Ther. 29, 1142–1153. https://doi.org/10.1111/cns.14096.

Wilmes, M., Pinto Espinoza, C., Ludewig, P., Stabernack, J., Liesz, A., Nicke, A., Gelderblom, M., Gerloff, C., Falzoni, S., Tolosa, E., Di Virgilio, F., Rissiek, B., Plesnilla, N., Koch-Nolte, F., Magnus, T., 2022. Blocking P2×7 by intracerebroventricular injection of P2×7-specific nanobodies reduces stroke lesions. J. Neuroinflamm. 19, 256 https://doi.org/10.1186/s12974-022-02601-z.

Zhang, X., Yu, Y., Lei, H., Cai, Y., Shen, J., Zhu, P., He, Q., Zhao, M., 2020. The Nrf-2/HO-1 signaling axis: a ray of hope in cardiovascular diseases. Cardiol. Res Pr. 2020, 5695723 https://doi.org/10.1155/2020/5695723.